Potential effects of POLR2H and DYNC1I2 on the immunity and prognosis of neuroblastoma

Yingxuan Ma
Department of General Surgery,Shanghai Children's Hospital, School of medicine, Shanghai Jiao Tong University.
Li Lu
Department of General Surgery,Shanghai Children's Hospital, School of medicine, Shanghai Jiao Tong University.
Zhi Li
Pathology Department,Shanghai Children's Hospital, School of medicine, Shanghai Jiao Tong University.
Weijue Xu
Department of General Surgery,Shanghai Children's Hospital, School of medicine, Shanghai Jiao Tong University.
Jiangbin Liu
Department of General Surgery,Shanghai Children's Hospital, School of medicine, Shanghai Jiao Tong University.
Ting Guo
Department of General Surgery,Shanghai Children's Hospital, School of medicine, Shanghai Jiao Tong University.
Yibo Wu
Department of General Surgery,Shanghai Children's Hospital, School of medicine, Shanghai Jiao Tong University.
Kezhe Tan
Department of General Surgery,Shanghai Children's Hospital, School of medicine, Shanghai Jiao Tong University.
Wei Wu
Department of General Surgery,Shanghai Children's Hospital, School of medicine, Shanghai Jiao Tong University.
Lulu Zheng
Department of General Surgery,Shanghai Children's Hospital, School of medicine, Shanghai Jiao Tong University.
Feilong Fan
Department of General Surgery,Shanghai Children's Hospital, School of medicine, Shanghai Jiao Tong University.
Zhenhua Gong (✉ gongzh1963@163.net)

Department of General Surgery,Shanghai Children's Hospital, School of medicine, Shanghai Jiao Tong University.

Zhibao Lv

Department of General Surgery,Shanghai Children's Hospital, School of medicine, Shanghai Jiao Tong University.

Research Article

Keywords: neuroblastoma, bioinformatics analysis, POLR2H, DYNC1I2, immune infiltration, overall survival

Posted Date: June 21st, 2022

DOI: https://doi.org/10.21203/rs.3.rs-1742595/v1

Abstract

Objective: The present study utilized bioinformatics techniques and data from the GEO, TARGET, and ArrayExpress databases to compare gene expression in INSS4 and INSS1 neuroblastomas (NBs), thereby identifying metabolites with different levels of expression and predicting the prognosis of patients with NB.

METHODS: Genes of patients with INSS4 and INSS1 NBs from the GEO database were screened, with those having | $\log_2$fold change (FC) | >3 and adjusted P <0.05 defined as being differentially expressed. These differentially expressed genes (DEGs) were screened to obtain clinical data and RNA sequence datasets from NB patients in the TARGET database. Univariate Cox proportional hazards regression analysis identified prognosis-related genes, which were incorporated into a prognosis model. Based on median risk scores, these patients were divided into high and low-risk groups. Their survival rates were compared, and ROC curves were used to analyze predictive values for NB. NB patients were also divided into two clusters by consensus clustering based on levels of POLR2H and DYNC1I2 expression. Immune infiltration analyses were performed using GSEA, ESTIMATE, CIBERSORT, and ssGSEA. Tumor tissue of 17 NB patients was used for experimental verification and their survival was compared.

Result: Analysis of three datasets identified 62 up-regulated genes and 163 down-regulated genes. The prognostic model predicted that the areas under the 3-year and 5-year survival curves were 0.786 and 0.817, respectively. Levels of expression of POLR2H and DYNC1I2 accounted for the highest percentage of risk scores and were included in follow-up analysis. Samples were consistently clustered according to their expression matrix. POLR2H was more highly expressed in cluster 2, whereas DYNC1I2 was more highly expressed in cluster 1. The survival rate of cluster 1 was significantly higher than that of cluster 2. Experimental verification in 17 NB patients showed that these patients could also be divided into two groups, which differed significantly in mortality hazard ratio (HR 9.37 P<0.05).

Conclusion: The expression of POLR2H and DYNC1I2 affects the immune microenvironment of NB and can affect patient prognosis. These factors can be used to refine clinical groupings, guide personalized treatment, and suggest new methods for the diagnosis and treatment of NB.

1. Introduction

Neuroblastoma (NB) is one of the most common malignancies in children, with these tumors being primarily derived from embryonic tumors of the sympathetic nervous system. The main sites are the sympathetic chain and the adrenal medulla (1). The Children's Oncology Group (COG) has estimated that 5-year overall survival (OS) rates are ≥ 95% in the low-risk group, 90–95% in the medium-risk group, and 50% in the high-risk group. Although NMYC amplification is an indicator of high risk and poor prognosis, with a 5-year OS rate < 50%, many patients with NB do not have BHLH Transcription Factor (NMYC) amplification (2). Although COG staging can roughly predict survival, its accuracy is highly dependent on

the results of clinician diagnosis and imaging using the International Neuroblastoma Staging System (INSS).

A comparison of patients with INSS stage I and INSS stage IV may provide information on the pathological characteristics of NB, may better stratify clinical risk, and be used to screen patients at high risk of death for personalized treatment. Differentially expressed genes (DEGs) in the GEO database were screened to include in a prognostic model for NB. This model was used to draw nomograms based on objective indicators, thereby simplifying the clinical diagnostic process and improving the ability to predict mortality risk.

To better understand the status of immune infiltration in patients with NB, patients were divided into two groups according to the expression of the proto-oncogene POLR2H and the tumor suppressor gene DYNC1I2. The two groups were compared using a bioinformatics method. The results showed that cluster 2, with high POLR2H and low DYNC1I2 expression, showed significantly higher mortality and higher immune infiltration than cluster 1, with low POLR2H and high DYNC1I2 expression.

2. Materials And Methods

2.1 Data acquisition and organization

Transcriptome data and clinical data for NB were obtained from the GEO, TARGET, and ArrayExpress databases. The GEO database (https://www.ncbi.nlm.nih.gov/geo/) is a microarray dataset, from which datasets GSE45547, GSE49710, and GSE16237 were selected.

Raw counts of RNA sequence data (level 3) for NB and corresponding clinical information were obtained from the TARGET dataset (https://ocg.cancer.gov/programs/target). Survival rates were determined by the Kaplan-Meier method and compared by log-rank tests. Factors associated with survival were determined by univariate Cox proportional hazards regression analyses, with results reported as hazard ratios (HRs) and 95% confidence intervals (CIs). All statistical analyses were performed using R software version, v4.1.3 (R Foundation for Statistics Computing, 2022), with $p < 0.05$ considered statistically significant. The validation set consisted of the microarray of the E-MTAB-8248 dataset obtained from the ArrayExpress database and the clinical data of NB patients.

2.2 Screening for differential genes

The differential expression of genes in the GEO datasets GSE45547, GSE49710, and GSE16237 were analyzed using the Limma package of R software. Adjusted P-values were analyzed by GEO to correct for false-positive results, with adjusted P-values <0.05 and $|\log_2 FC| > 3$ defined as the threshold for differential expression of mRNAs.

2.3 Prognostic model

Clinical data were downloaded from the TARGET database, with samples showing complete expression data and survival dates being retained. A DSN was introduced to analyze prognosis-related genes, and a prognostic model was constructed following univariate Cox proportional hazards regression analyses, with $P < 0.05$ considered meaningful. Survival-related genes were further analyzed by Lasso regression analysis; the λ value with the smallest error was selected and the corresponding gene was retained. The validity of the prognostic model was assessed using the E-MTAB-8248 dataset in the ArrayExpress database.

The risk score for each sample was calculated based on the regression coefficient (β) of each gene and its expression in each sample. Samples were divided into high-risk and low-risk groups according to the median risk score. The differences between the two groups were determined by the Kaplan-Meier method. A receiver operating characteristics (ROC) curve was drawn, with the predictive ability of the genetic model determined by calculating the area under the ROC curve (AUC). AUCs closer to 1 were associated with smaller P-values and higher predictive power.

Although COG staging can roughly predict survival, its accuracy is highly dependent on the clinician judgment and the results of imaging tests, making it somewhat subjective. Based on clinical information about patients with NB and retrospective studies of prognostic models, a nomogram predictive of prognosis was constructed based on age, gender, MYCN, MKI, and risk scores.

2.4 Tumor immunity

Immune cell infiltration in 142 NB patients in the TARGET dataset was obtained through TCGA (https://portal.gdc.cancer.gov). The correlation between risk score of the prognosis model and infiltration of various immune cells was calculated. The expression of subsets of putative RNA transcripts (CIBERSORT) was determined to evaluate the abundance of cell types in the mixed cell population. The CIBERSORT gene signature matrix, called LM22, consists of 547 genes and distinguishes among 22 human hematopoietic cell phenotypes, including seven T cell types, naive and memory B cells, plasma cells, NK cells, and myeloid subsets.

The immune cell profile of each of the 142 samples in the TARGET dataset was determined using CIBERSORT, with the number of sequences set at 100. The correlations between the expression of 12 prognosis-related genes and immune cell infiltration were determined by Pearson correlation analysis and used to draw correlation heatmaps.

2.5 Consensus clustering based on POLR2H and DYNC1I2

Because the prognosis of NB patients with different gene expression levels varied, unsupervised clustering analysis was performed to identify differential gene expression. The patients were divided into two clusters. None of the 12 prognosis-related genes were highly correlated with infiltration of immune cells. POLR2H and DYNC1I2 accounted for the highest percentage of risk scores and were included in subsequent analysis. TARGET-NBL samples were clustered according to their expression matrices and

survival curves were drawn (3). Sankey diagrams represented the relationships of the two clusters with clinical stage and patient prognosis.

2.6 Differential gene enrichment analysis

Based on the comparisons between clusters 1 and 2, the thresholds were adjusted to P <0.05 and $|\log_2 FC| > 1$, and the differentially expressed genes were analyzed by enhancement.

Gene Ontology (GO) is widely used to annotate functional genes and is divided into three parts: molecular function, biological processes, and cellular components. To better understand the effect of target genes on tumors, the ClusterProfiler package in R was used to analyze the GO function of the underlying mRNAs.

GSEA was run using the R package cluster profile to determine significant functional differences between the two clusters. Significantly enriched pathways were defined as those with a (| normalized enrichment score (NES) |) > 1, a P-value <0.05, and an FDRq value <0.25 (4).

2.7 Immune infiltration analysis

ESTIMATE is a method of determining the ratio of stromal cells to immune cells based on the gene expression signature of a tumor sample. The tumor microenvironment (TME) in each NB patient was evaluated, as along with the stromal score (stroma content), immune score (degree of immune cell infiltration), ESTIMATE score (synthetic markers of stroma and immunity), and tumor purity using the R package (5).

CIBERSORT is a method of calculating cell composition based on an expression profile. This algorithm was used to calculate the proportion of 22 immune cells in each patient, with the sum of the proportions of the 22 immune cell fractions in each sample being 1 (6).

The degree of infiltration of 28 types of immune cells was calculated based on the level of gene expression in the 28 published immune cell genomes using the R Package GSVA Single-Sample Gene Set Concentration Analysis (ssGSEA) method (7).

2.8 Sampling and real-time PCR

After obtaining informed consent from the children of patients with NB and approval from the Institutional Review Board of Shanghai Children's Hospital (batch number: 2022R036-E01), 17 NB specimens were collected from our hospital from 2016 to 2019. Total RNA was extracted using TRIzol reagent (Invitrogen), and cDNA was synthesized using the Prime Script RT kit (TaKaRa). RT-qPCR was performed using specific primers (Table 1) and SYBR Prime Script RT-PCR kits (TaKaRa), according to the manufacturer's protocol.

Table 1. RT-PCR primers (5’→3’)

PWK0405-H-POLR2H-F	CCAGGGCTGACCAGTTTGAGTATG
PWK0406-H-POLR2H-R	AGGCGTGTTGCTGCTTCAGTAG
PWK0407-H-DYNC1I2-F	CCATCCTCCAAATCTGTGAGCACTC
PWK0408-H-DYNC1I2-R	GTCCTCGTCCCAAATCGGAATCTG
Human GAPDH primer F	GCACCGTCAAGGCTGAGAAC
Human GAPDH primer R	TGGTGAAGACGCCAGTGGA

F, forward; R, reverse; GAPDH was used as an internal control.

2.9 Statistical Analysis

All statistical analyses were performed using R (4.1.2) and SPSS (25.0) software. Box plot analyses were performed using the Wilcoxon rank-sum test. Correlation analysis was performed using Spearman's coefficient. Lasso regression analysis was performed to evaluate the clinical characteristics affecting the clusters. Survival curves were constructed using the Kaplan–Meier method and compared by log-rank tests. All tests were two-sided, with P-values <0.05 considered statistically significant.

3. Results

3.1 Differential gene expression

The GSE45547, GSE49710, and GSE16237 datasets downloaded from the GEO database were normalized (Figures 1A, 1B) and screened for genes differentially expressed by INSS IV and INSS I NBs. Genes with adjusted P-values <0.05 and $|\log_2 FC| > 3$ were considered differentially expressed. A total of 62 genes were upregulated and 163 downregulated in NBs compared with adjacent normal tissue, as shown by volcano plots (Figure 1C) and heatmaps (Figure 1D).

3.2 Prognostic regression model

The ability of 53 prognosis-related genes to affect survival was determined by Kaplan-Meier analysis, and a Forest plot was drawn (Fig. 2A). Survival-related genes were further analyzed by lasso regression analysis to reduce interactions between variables (Fig. 2B). The λ value corresponding to the smallest error was selected and the corresponding gene was retained (Fig. 2C). Twelve genes were identified (Fig. 2D), and their ROC curves were plotted (Fig. 2E).

Table 2. Areas under the curve (AUC) of prognosis-related genes

Gene	AUC
STK33	0.67
EIF2B2	0.68
PHIP	0.32
PTBP2	0.28
RUVBL1	0.71
POLR2H	0.73
TIA1	0.30
PAGE5	0.68
ANKRD60	0.65
DYNC1I2	0.25
SCN3A	0.26
NREP	0.27

The results of the lasso regression were integrated into the prognostic function to build and validate a prognostic model. A heat map scatter plot shows the distribution of risk scores, the survival status of each subject, and gene expression patterns (Fig. 3A). During follow-up, most of the patients in the high-risk group died and most of the patients in the low-risk group survived (Fig. 3B). The heatmap showed that six metabolism-related genes were highly expressed in the high-risk group and six metabolism-related genes were highly expressed in the low-risk group (Fig. 3C).

Risk score=1.1580*POLR2H+1.1437*ANKRD60+（-0.8321）* DYNC1I2+0.4468* EIF2B2+ 0.3572* RUVBL1+（-0.3006）*NREP+0.2128* STK33+（-0.2081）* PHIP+0.1755* SCN3A+（-0.0673）* PTBP2+0.0589* PAGE5+（-0.0031）* TIA1.

The differences between the two groups were compared by the Kaplan-Meier method curve. The HR for low vs. high risk was found to be 0.31 (95% CI: 0.17-0.55), with a P value <0.001, showing that the grouping was meaningful (Fig. 3D). The ROC curves of the survival model indicated that the 3-year and 5-year AUCs were 78.6% and 81.7%, respectively (Fig. 3E).

Prognostic Model Validation

The prognostic model was externally validated using the E-MTAB-8248 dataset from the ArrayExpress database. These patients were successfully divided into high-risk and low-risk groups based on their risk scores (Fig. 4A-D). The HR for low vs high risk was 0.23 (95% CI 0.11-0.48, P <0.001), indicate that the model was valid. The 3-year and 5-year AUCs of the survival model were 72.1% and 74.7%, respectively (Fig. 4E).

Nomogram

Multivariate Cox survival analysis compared the effects of gender, age (<12 months vs. ≥12 months), MYCN amplification (non-amplified vs. amplified), ploidy (diploid vs. hyperdiploid), and MKI (low, medium, high) on 92 patients with complete data in the TARGET-NB dataset were retained. The HRs for the predictive model, ploidy, age, MKI, and COG score were 1.664 (95% CI 1.417-1.955, P <0.001), 0.424 (95% CI 0.23-0.784; P = 0.006), 16.014 (95% CI 2.201-116.519; P = 0.006), 1.771 (95% CI 1.205-2.602; P = 0.004) and 8.643 (95% CI 1.437-51.998; P = 0.018), respectively, for OS (Fig. 5A).

The nomogram containing the risk scores of the metabolic gene signature for OS prediction was found to have a C-index of 0.766, indicating high prediction accuracy (Fig. 5B). A calibration curve showed that the 5-year OS predicted by the nomogram was very close to the actual 5-year OS (Fig. 5C).

Risk score and immune correlation analysis

The correlation between risk score and immune cell infiltration into NBs was assessed by Spearman analysis using data from the TIMER database (http://timer.cistrome.org/) to determine if risk scores were associated with tumor immunity (Fig. 6A-F). Risk score was significantly negatively correlated with NK cell (-0.50) and myeloid dendritic cell (-0.41) infiltration, but was significantly positively correlated with infiltration of common lymphoid progenitor cells (0.37), B cells (0.354), and CD4+ Th1 T cells (0.494).

The abscissa in each panel represents the distribution of risk scores, and the ordinate represents the distribution of immune scores. The density curve on the right represents the trend in the distribution of immune scores, and the upper-density curve represents the trend in the distribution of risk scores. The value at the top represents the p-value of the correlation coefficient.

Table 3. risk_score

	Pearson correlation coefficient	Sig.
NK cell_QUANTISEQ	-0.50**	0
Myeloid dendritic cell_QUANTISEQ	-0.41**	0
uncharacterized cell_QUANTISEQ	0.42**	0
Common lymphoid progenitor_XCELL	0.37**	0
B cell plasma_XCELL	0.35**	0
T cell CD4+ Th1_XCELL	0.49**	0
Macrophage M0_CIBERSORT	0.25**	0.003
T cell CD4+ Th2_XCELL	0.25**	0.003
T cell regulatory (Tregs)_QUANTISEQ	-0.24**	0.004
T cell CD4+ (non-regulatory)_QUANTISEQ	-0.23**	0.006
Macrophage M0_CIBERSORT-ABS	0.22**	0.008
Neutrophil_QUANTISEQ	0.22**	0.01
Macrophage M2_CIBERSORT	-0.20*	0.015
T cell CD8+_TIMER	-0.20*	0.017
Macrophage M2_CIBERSORT-ABS	-0.20*	0.017
Mast cell_XCELL	-0.18*	0.032

Tumor immunity

The immune cell profile of each sample in TARGET was assessed by CIBERSORT, with the number of sequences set at 100 (6) (Fig. 7A). The correlation between the 12 genes in the predictive model and the infiltration of immune cells was assessed by creating a correlation heatmap showing the Pearson correlation coefficients of the sample immune cells selected by CIBERSORT and the 12 prognosis-related genes (Fig. 7B).

Because the prognosis of NB patients was related to differences in gene expression levels and none of the 12 prognosis-related genes was highly correlated with immune cells, the protooncogene POLR2H and the tumor suppressor gene DYNC1I2, which account for the highest proportion of risk scores, were included in subsequent analyses. The 142 TARGET-NBL samples were uniformly clustered according to the expression matrix and the samples were split into two clusters. Cluster 1 consisted of 64 patients with low POLR2H and high DYNC1I2 expression, whereas cluster 2 consisted of 78 patients with high POLR2H and low DYNC1I2 expression (Fig. 8A). Because these two genes showed opposite trends in the two clusters, their correlation was assessed, with Spearman correlation analysis showing that POLR2H and DYNC1I2 expression were negatively correlated (-: p = 1.6e-4 r = -0.31) (Fig. 8B).

Kaplan-Meier analysis showed that the survival curves of patients in the two clusters differed significantly (Fig. 8C), with the risk of death being significantly lower in cluster 1 than in cluster 2 (HR = 2.68, P <0.001). A Sankey diagram shows the relationship between clinical data and survival of each patient (Fig. 8D).

Differential gene enrichment analysis

To explore the differentially expressed genes and their functions in the two groups of patients, differential analysis of patients in clusters 1 and 2 was performed using as criteria $|\log_2 FC|>1$ and adjusted $P<0.05$. This analysis showed that 52 genes were up-regulated and 20 were down-regulated (Fig. 9A). GO enrichment analysis showed that the main enrichments were in categories that included neurotransmitter transport, regulation of neurotransmitter levels, transport vesicles, synaptic vesicle cycle, vesicle-mediated transport in synapses, response to xenobiotic stimuli, exocytic vesicles, monoamine transport, amine transport, synaptic vesicles, organic hydroxy compound transport, exocytosis, cell junction assembly, signal release, axon development, catecholamine transport, regulation of exocytosis, responses to metal ions, axonogenesis, synapse organization, and metal ion transmembrane transporter activity (Fig. 9B).

Tumor purity

To investigate the role of tumor immunity in NB patients, ESTIMATE was performed to evaluate stromal and immune cell fractions. Cluster 1 had higher tumor purity than cluster 2, whereas cluster 2 had a higher interstitial score (matrix content), immune score (degree of immune cell infiltration), and ESTIMATE score (matrix and immune synthetic marker). The differences were not statistically significant, however, possibly because the sample sizes were small (Fig. 10).

Comparison of immune infiltration

CIBERSORT analysis showed that the proportion of M1 macrophages was higher in cluster 2 than in cluster and that dendritic cells in cluster 2 were dormant (Fig. 11A, Fig. 13D). In comparison, ssGSEA showed that the proportions of $CD56^{bright}$ natural killer cells, MDSCs and plasmacytoid dendritic cells were higher, and the proportion of immature dendritic cells lower, in cluster 2 than in cluster 1 (Fig. 11B, 13E).

GSEA enrichment analysis

Functional differences between the two clusters were assessed by GSEA of all differentially expressed genes (Cluster 2 vs. Cluster 1). Many important pathways found to be enriched in the MSigDB collection (h.all.v7.4.symbols.GMT) were validated in cluster 1 of the E-MTAB-8248 dataset (Fig.12A, Fig. 13F), including genes associated with protein secretion, bile acid metabolism, UV response DN, and hedgehog signaling. Genes enriched in cluster 2 (Fig. 12B, Fig. 13G) included those associated with E2F targeting, the MYC target V2, the G2M checkpoint, and MYC target V1.

Table 4. TARGET-NBLGSEA results

Group1

NAME	SIZE	NES	NOM p-val	FDR q-val	RANK AT MAX	LEADING EDGE
HALLMARK PROTEIN SECRETION	95	1.79	0.00	0.00	6596	tags=60%, list=34%, signal=90%
HALLMARK BILE ACID METABOLISM	112	1.71	0.00	0.01	3963	tags=35%, list=20%, signal=43%
HALLMARK UV RESPONSE DN	141	1.63	0.00	0.01	3511	tags=40%, list=18%, signal=49%
HALLMARK MITOTIC SPINDLE	198	1.61	0.00	0.01	5138	tags=37%, list=26%, signal=50%
HALLMARK HEDGEHOG SIGNALING	36	1.60	0.01	0.01	4004	tags=47%, list=20%, signal=59%

Group2

NAME	SIZE	NES	NOM p-val	FDR q-val	RANK AT MAX	LEADING EDGE
HALLMARK TNFA SIGNALING VIA NFKB	199	-3.42	0.00	0.00	2838	tags=53%, list=14%, signal=62%
HALLMARK MYC TARGETS V2	58	-3.02	0.00	0.00	2903	tags=57%, list=15%, signal=67%
HALLMARK EPITHELIAL MESENCHYMAL TRANSITION	198	-2.83	0.00	0.00	3451	tags=55%, list=18%, signal=66%
HALLMARK INFLAMMATORY RESPONSE	200	-2.47	0.00	0.00	3342	tags=44%, list=17%, signal=52%
HALLMARK INTERFERON GAMMA RESPONSE	198	-2.39	0.00	0.00	4668	tags=50%, list=24%, signal=65%
HALLMARK INTERFERON ALPHA RESPONSE	95	-2.28	0.00	0.00	3260	tags=45%, list=17%, signal=54%
HALLMARK ALLOGRAFT REJECTION	196	-2.18	0.00	0.00	5383	tags=48%, list=27%, signal=65%
HALLMARK MYC TARGETS V1	196	-2.17	0.00	0.00	6321	tags=50%, list=32%, signal=73%
HALLMARK P53 PATHWAY	195	-2.17	0.00	0.00	2971	tags=37%, list=15%, signal=43%
HALLMARK HYPOXIA	197	-2.07	0.00	0.00	2917	tags=35%, list=15%, signal=40%
HALLMARK ANGIOGENESIS	36	-2.01	0.00	0.00	3232	tags=50%, list=16%, signal=60%
HALLMARK IL2 STAT5 SIGNALING	198	-1.90	0.00	0.00	3967	tags=41%, list=20%, signal=51%
HALLMARK APOPTOSIS	160	-1.89	0.00	0.00	3919	tags=39%, list=20%, signal=48%
HALLMARK IL6 JAK STAT3 SIGNALING	87	-1.85	0.00	0.00	5668	tags=60%, list=29%, signal=84%

HALLMARK REACTIVE OXYGEN SPECIES PATHWAY	49	-1.84	0.00	0.00	5260	tags=43%, list=27%, signal=58%
HALLMARK DNA REPAIR	148	-1.72	0.00	0.00	4456	tags=36%, list=23%, signal=47%
HALLMARK UNFOLDED PROTEIN RESPONSE	109	-1.70	0.00	0.00	2425	tags=25%, list=12%, signal=28%
HALLMARK KRAS SIGNALING UP	198	-1.61	0.00	0.00	2553	tags=27%, list=13%, signal=31%
HALLMARK UV RESPONSE UP	156	-1.60	0.00	0.01	3770	tags=35%, list=19%, signal=43%
HALLMARK MYOGENESIS	199	-1.50	0.00	0.01	3904	tags=30%, list=20%, signal=37%
HALLMARK TGF BETA SIGNALING	54	-1.49	0.02	0.02	3020	tags=37%, list=15%, signal=44%
HALLMARK MTORC1 SIGNALING	196	-1.46	0.00	0.02	5551	tags=40%, list=28%, signal=55%
HALLMARK ESTROGEN RESPONSE EARLY	198	-1.33	0.00	0.06	3399	tags=30%, list=17%, signal=36%
HALLMARK ESTROGEN RESPONSE LATE	197	-1.33	0.04	0.06	3834	tags=32%, list=20%, signal=40%
HALLMARK GLYCOLYSIS	198	-1.28	0.01	0.08	2552	tags=20%, list=13%, signal=22%
HALLMARK COAGULATION	138	-1.22	0.06	0.12	3132	tags=26%, list=16%, signal=31%
HALLMARK E2F TARGETS	198	-1.21	0.06	0.13	5925	tags=38%, list=30%, signal=54%
HALLMARK NOTCH SIGNALING	32	-1.15	0.23	0.19	3802	tags=34%, list=19%, signal=43%
HALLMARK COMPLEMENT	200	-1.14	0.10	0.20	4563	tags=36%, list=23%, signal=46%

HALLMARK CHOLESTEROL HOMEOSTASIS	73	-1.06	0.30	0.34	2636	tags=25%, list=13%, signal=28%
HALLMARK OXIDATIVE PHOSPHORYLATION	185	-1.06	0.26	0.35	5513	tags=38%, list=28%, signal=52%
HALLMARK G2M CHECKPOINT	194	-1.02	0.40	0.44	4183	tags=24%, list=21%, signal=30%

E-MTAB-8248 Validation of Differences in Immune Characteristics in the Two Clusters

A total of 223 NB samples from E-MTAB-8248 in the ArrayExpress database were divided into two clusters, in the same manner as the division of the TCGA dataset (Fig. 13A). The distribution of POLR2H and DYNC1I2 expression in the two clusters was similar to that observed in the TCGA dataset. The expression of POLR2H and DYNC1I2 showed a significant negative correlation (R = -0.60, P <0.001; Fig. 13B). Kaplan-Meier analysis HR=0.23 P<0.001(Fig. 13C), and analysis by CIBERSORT (Fig. 13D), ssGSEA (Figs. 13D, 13E) and GSEA (Figs. 13F, 13G, Table 5) yielded similar results.

Table 5. E-MTAB-8248GSEA results

Group1

NAME	SIZE	NES	NOM p-val	FDR q-val	RANK AT MAX	LEADING EDGE
HALLMARK PROTEIN SECRETION	91	1.88	0.00	0.00	5166	tags=45%, list=26%, signal=61%
HALLMARK HEDGEHOG SIGNALING	35	1.88	0.00	0.00	3785	tags=43%, list=19%, signal=53%
HALLMARK UV RESPONSE DN	133	1.60	0.00	0.04	4484	tags=37%, list=23%, signal=47%
HALLMARK BILE ACID METABOLISM	112	1.49	0.00	0.09	4341	tags=39%, list=22%, signal=50%
HALLMARK HEME METABOLISM	183	1.47	0.00	0.09	4784	tags=34%, list=24%, signal=44%
HALLMARK APOPTOSIS	155	1.37	0.03	0.17	5363	tags=41%, list=27%, signal=55%
HALLMARK FATTY ACID METABOLISM	151	1.35	0.03	0.16	6111	tags=45%, list=31%, signal=65%

Group2

NAME	SIZE	NES	NOM p-val	FDR q-val	RANK AT MAX	LEADING EDGE
HALLMARK E2F TARGETS	179	-2.19	0.00	0.00	5256	tags=46%, list=26%, signal=62%
HALLMARK MYC TARGETS V2	52	-2.16	0.00	0.00	5509	tags=60%, list=28%, signal=82%
HALLMARK G2M CHECKPOINT	178	-2.14	0.00	0.00	5039	tags=47%, list=25%, signal=62%
HALLMARK MYC TARGETS V1	180	-1.41	0.01	0.08	5905	tags=34%, list=30%, signal=48%

Verification of clinical samples

Levels of expression of POLR2H and DYNC1I2 in primary NBs

The levels of expression of POLR2H and DYNC1I2 in tumor tissue of 17 patients with NB were analyzed by RT-qPCR. Based on the expression of POLR2H and DYNC1I2 mRNAs, the patients could be divided into two clusters, with POLR2H expression being higher and DYNC1I2 significantly lower (P <0.001) in group 2 than in group (Fig. 15A, 15C). Kaplan-Meier analysis showed that the risk of death was significantly lower in group 1 than in group 2 (HR = 9.37 P <0.05) (Fig. 15B). A Sankey diagram shows the relationship between clinical features and prognosis in the 17 patients with NB (Fig. 15D).

Discussion

The prognostic model designed in the present study showed the involvement of several protooncogenes, such as POLR2H, ANKRD60, EIF2B2, PAGE5, STK33, and RUVBL1, and several tumor suppressor genes, such as DYNC1I2, NREP, PHIP, PTBP2, TIA1, and SCN3A. Risk score could be calculated using the formula 1.1580*POLR2H+1.1437*ANKRD60+ (-0.8321)* DYNC1I2+0.4468* EIF2B2+ 0.3572* RUVBL1+ (-0.3006)*NREP+0.2128* STK33+(-0.2081)* PHIP+0.1755* SCN3A+(-0.0673)* PTBP2+0.0589* PAGE5+ (-0.0031)* TIA1.

POLR2H, or DNA-directed RNA polymerase II subunit H, also called hRPB17 or RPB8), is one of three eukaryotic RNA polymerases. These complex multisubunit enzymes play a central role in the transcription of nuclear genes. POLR2H is rarely expressed in NB but is significantly upregulated in prostate cancer (8). In addition, it has been found to be present in extrachromosomal circular DNA (eccDNA), the levels of which are increased in cancer cells and overlap with oncogenic and drug-resistant genes. POLR2H has been associated with endogenous microDNA [9] and may act as a proto-oncogene in NB, consistent with our findings.

Co-immunoprecipitation has shown that DYNC1I2, or dynein cytoplasmic 1 intermediate chain 2, interacts with TMEM39A in mammalian cells. TMEM39A is an evolutionarily conserved protein involved in promoting proper lysosome positioning and accumulation, which are important for regulation of mTOR

signaling, autophagy initiation, and immune-cell responses under a variety of physiological and pathological conditions (10). Changes in DYNC1I2 expression may be key to inducing immune responses in NB.

Although few studies have assessed the role of ANKRD60 (ankyrin repeat domain 60, also called chromosome 20 open reading frame 86,a recent Korean study found that it may be related to human growth and development. In addition, chromosome 20 is involved in many diseases and is abnormally expressed in patients with myelodysplastic disease and myelodysplastic syndrome (11, 12). The location of ANKRD60 on chromosome 20 suggests its association with NB tumor growth.

EIF2B2, or eukaryotic translation initiation factor 2B subunit beta, is a master regulator of global protein synthesis in all types of cells (13), and PAGE5, or PAGE family member 5, also called cancer-testis antigen 16 (CT16) is a member of a family of proteins expressed in various tumors and some fetal and reproductive tissues. PAGE5 has been found to regulate the expression of apoptotic and anti-apoptotic genes and promote cell survival (14). In addition, STK33, or serine/threonine kinase 33, has been shown to promotes the growth and progression of human pancreatic neuroendocrine tumors by activating the PI3K/AKT/mTOR pathway (15). STK33 overexpression was found to promote the proliferation, migration, invasion, and growth of pancreatic ductal adenocarcinoma, with STK33 depletion having the opposite effects (16), suggesting that STK33 may promote tumor growth in NB.

RUVBL1, or RuvB-like AAA ATPase 1, has been associated with poor prognosis and a higher relapse rate in patients with diffuse large B-cell lymphoma (17). In addition, high expression of RuvBL1 in lung cancer was associated with a poor overall prognosis (18). NREP, or neuronal regeneration related protein, may be involved in neural function, including the promotion of axonal regeneration. NREP may also function in cellular differentiation and has been shown to promote gastric cancer metastasis (19). Its role in NB, however, remains unclear.

PHIP, or pleckstrin homology domain interacting protein, has been shown to play an important role in regulating the site-specific initiation of DNA replication and cell cycle progression (20). Upregulation of PTBP2, or polypyrimidine tract binding protein 2, was found to induce neuronal differentiation (21), suggesting that this protein may induce the differentiation of NB cells and play a protective role. TIA1, or TIA1 cytotoxic granule associated RNA binding protein may be involved in the induction of apoptosis, as it preferentially recognizes poly(A) homopolymers and induces DNA fragmentation in CTL targets. The expression of TIA1 was recently shown to be down-regulated in gastric cancer tissues and to promote gastric cancer GC cell apoptosis (22). Although SCN3A, or sodium voltage-gated channel alpha subunit 3, was found to have protective activity, its high expression in predictive models has been associated with increased risk, which is related to sodium channels and epilepsy (23, 24).

Established prognostic models and nomograms based on these 12 genes can be used to predict survival in NB patients and further develop individualized diagnostic and treatment plans. The correlation analysis between risk score and tumor immunity in our predictive model suggested that high-risk NBs are infiltrated by low numbers of NK cells, myeloid dendritic cells (mDCs), general lymphoid precursor cells,

and B cells, and by high numbers of CD4 + Th1 T cells. NK cell cytotoxic activity has been shown to play a major role in natural immunologic defenses against malignancies (25). Moreover, intravenous injection of a combined vaccine composed of mDCs and plasmacytoid dendritic cell (pDC) into tumor-bearing nude mice was found to significantly inhibit subcutaneous tumor growth and to induce necrosis and apoptosis within the tumor tissue (26). Lymphoid progenitor cells and B cells were also shown to play roles in the progression of other tumors (27, 28). Higher levels of interferon (IFN)-γ-expressing CD4+ T (Th1) cells in patients with cancer have been associated with better prognosis, suggesting that Th1 cells are involved in controlling tumor regression (29-31). The elevated numbers of CD4 + Th1 T-cells in the high-risk group in the present study suggest that these cells do not play a protective role in NB. Taken together, however, these findings indicate that immune responses play an important role in the death of patients with NB.

To more accurately assess the immune status of NB patients, the proto-oncogene POLR2H and the tumor suppressor gene DYNC1I2 were included in follow-up studies. NB patients were divided into two clusters based on consensus, with Cluster 1 consisting of patients with low POLR2H and high DYNC1I2 expression and Cluster 2 consisting of patients with high POLR2H and low DYNC1I2 expression. Kaplan-Meier analysis showed that the survival rate was significantly higher in cluster 1 than in cluster 2, and that cluster 1 tumors were purer.

GO enrichment analysis of NB tissue showed enrichment of genes associated with neurotransmitter transport, regulation of neurotransmitter levels, transport vesicles, synaptic vesicle cycle, vesicle-mediated transport in synapses, responses to xenobiotic stimuli, exocytic vesicles, monoamine transport, amine transport, synaptic vesicles, organic hydroxy compound transport, exocytosis, cell junction assembly, signal release, axon development, catecholamine transport, regulation of exocytosis, response to metal ions, axonogenesis, synapse organization, and metal ion transmembrane transporter activity. These features may be closely related to the progression of NB.

CIBERSORT analysis showed a high proportion of dormant M1 macrophages and a low percentage of dendritic cells in cluster 2, whereas ssGSEA analyses showed high proportions of $CD56^{bright}$ NK cells, MDSCs, and plasmacytoid dendritic cells, and a low proportion of immature dendritic cells, in cluster 2. Th1 cells polarize macrophages toward the M1 phenotype, whereas Th2 cells polarize macrophages toward the M2 phenotype. Evaluation of macrophage phenotype enrichment in NB showed that M1 macrophages are significantly enriched in NBs without MYCN amplification, whereas M2 macrophages are more abundant in NBs with MYCN amplification (31). CD56 NK cells are dysfunctional and prevalent in higher-stage tumors and correlate inversely with survival of melanoma patients (32, 33). Administration of low dose doxorubicin (DOX) or dopamine (DA) has been shown to eliminate MDSCs, alleviate immunosuppression and improve immune responses against NB tumor cells (34). In addition, Toll-like receptor (TLR)-activated plasmacytoid dendritic cells (pDCs) were found to strongly increase the cytotoxic activities of NK cells in high-risk NB patients undergoing immunotherapy (35). These results suggest that immunotherapy may be highly effective in cluster 2 NB patients.

GSEA enrichment analysis on a gene set (h.all.v7.4.symbols.GMT) in two groups of patients identified pathways associated with Hedgehog signaling, E2F TARGETS, G2M CHECKPOINT and MYC TARGETS. Hedgehog signaling has been shown to accelerate the development of NB (36, 37), and E2F TARGETS were found to interact with NMYC and promote NB growth via BIRC5 (baculovirus IAP repeat-containing 5), also known as survivin (38, 39). G2M CHECKPOINT and MYC TARGETS, which are related to cell-cycle functions, were found to be negative hallmarks and play important roles in other tumors (40). Further investigation is required to determine if these pathways are upregulated in NB.

Analysis of PCR results in 17 patients with NB at Shanghai Children's Hospital resulted in their classification into two groups based on POLR2H and DYNC1I2 expression levels. Patients with high DYNC1I2 and low POLR2H expression had significantly better prognosis and a significantly higher survival rate than patients with low DYNC1I2 and high POLR2H expression.

The present study had several limitations, including its retrospective design. Prospective studies are therefore needed to avoid the analytical biases associated with retrospective studies. In addition, this study did not analyze the levels of expression of POLR2H and DYNC1I2 at the protein level or determine the direct mechanisms by which POLR2H and DYNC1I2 are involved in anti-tumor immunity.

A nomogram that includes the levels of expression of POLR2H, ANKRD60, DYNC1I2, EIF2B2, RUVBL1, NREP, STK33, PHIP, SCN3A, PTBP2, PAGE5 and TIA1 mRNAs, along with age, gender, MKI, and NMYC, can be used to predict the survival rate of NB patients. In addition, the expression of POLR2H and DYNC1I2 was found to alter the immune microenvironment of NBs and can affect the prognosis of patients with this disease. Clinical grouping of NB patients based on their levels of expression of POLR2H and DYNC1I2 can guide personalized treatment, and may suggest new methods for the diagnosis and treatment of NB.

Declarations

Conflict of Interest

The authors declare that they have no conflict of interest.

Author Contributions

YM and ZG conceived the idea for the article and performed data analysis, data interpretation, and manuscript preparation. LL, FF, WW, ZLv, WX and LJ performed the data acquisition, ZL, GT,LZ, KT, and YW contributed to the critical review of the intellectual content of this manuscript. All authors reviewed the manuscript.

Funding

None.

Acknowledgments

We thank our colleagues and hospital for their help with this study during the COVID-19 pandemic.

References

1. Maris JM. Recent advances in neuroblastoma. N Engl J Med (2010) 362:2202–11. doi: 10.1056/NEJMra0804577
2. Moreno L, Guo D, Irwin MS, Berthold F, Hogarty M, Kamijo T, et al. A nomogram of clinical and biologic factors to predict survival in children newly diagnosed with high-risk neuroblastoma: An International Neuroblastoma Risk Group project. Pediatr Blood Cancer (2021) 68:e28794. doi: 10.1002/pbc.28794
3. Wilkerson MD, Hayes DN. ConsensusClusterPlus: a class discovery tool with confidence assessments and item tracking. Bioinformatics (2010) 26:1572–3. doi: 10.1093/bioinformatics/btq170
4. Yu G, Wang LG, Han Y, He QY. clusterProfiler: an R package for comparing biological themes among gene clusters. Omics (2012) 16:284–7. doi: 10.1089/omi.2011.0118
5. Yoshihara K, Shahmoradgoli M, Martínez E, Vegesna R, Kim H, Torres-Garcia W, et al. Inferring tumour purity and stromal and immune cell admixture from expression data. Nat Commun (2013) 4:2612. doi: 10.1038/ncomms3612
6. Newman AM, Liu CL, Green MR, Gentles AJ, Feng W, Xu Y, et al. Robust enumeration of cell subsets from tissue expression profiles. Nat Methods (2015) 12:453–7. doi: 10.1038/nmeth.3337
7. Bindea G, Mlecnik B, Tosolini M, Kirilovsky A, Waldner M, Obenauf AC, et al. Spatiotemporal dynamics of intratumoral immune cells reveal the immune landscape in human cancer. Immunity (2013) 39:782–95. doi: 10.1016/j.immuni.2013.10.003
8. Fan S, Liang Z, Gao Z, Pan Z, Han S, Liu X, et al. Identification of the key genes and pathways in prostate cancer. Oncol Lett (2018) 16:6663–9. doi: 10.3892/ol.2018.9491
9. Paulsen T, Shibata Y, Kumar P, Dillon L, Dutta A. Small extrachromosomal circular DNAs, microDNA, produce short regulatory RNAs that suppress gene expression independent of canonical promoters. Nucleic Acids Res (2019) 47:4586–96. doi: 10.1093/nar/gkz155
10. Luo S, Wang X, Bai M, Jiang W, Zhang Z, Chen Y, et al. The conserved autoimmune-disease risk gene TMEM39A regulates lysosome dynamics. Proc Natl Acad Sci U S A (2021) 118:e2011379118. doi: 10.1073/pnas.2011379118
11. Deloukas P, Matthews LH, Ashurst J, Burton J, Gilbert JG, Jones M, et al. The DNA sequence and comparative analysis of human chromosome 20. Nature (2001) 414:865–71. doi: 10.1038/414865a
12. Kim JJ, Lee HI, Park T, Kim K, Lee JE, Cho NH, et al. Identification of 15 loci influencing height in a Korean population. J Hum Genet (2010) 55:27–31. doi: 10.1038/jhg.2009.116
13. Herrero M, Daw M, Atzmon A, Elroy-Stein O. The energy status of astrocytes is the Achilles' heel of eIF2B-leukodystrophy. Cells (2021) 10:1858. doi: 10.3390/cells10081858

14. Nylund C, Rappu P, Pakula E, Heino A, Laato L, Elo LL, et al. Melanoma-associated cancer-testis antigen 16 (CT16) regulates the expression of apoptotic and antiapoptotic genes and promotes cell survival. PLoS One (2012) 7:e45382. doi: 10.1371/journal.pone.0045382
15. Zhou B, Xiang J, Zhan C, Liu J, Yan S. STK33 promotes the growth and progression of human pancreatic neuroendocrine tumour via activation of the PI3K/AKT/mTOR pathway. Neuroendocrinology (2020) 110:307 – 20. doi: 10.1159/000501829
16. Kong F, Kong X, Du Y, Chen Y, Deng X, Zhu J, et al. STK33 promotes growth and progression of pancreatic cancer as a critical downstream mediator of HIF1α. Cancer Res (2017) 77:6851–62. doi: 10.1158/0008-5472.Can-17-0067
17. Lone M, Shadang M, Akhter Q, Kumar M, Mallick S, Gogia A, et al. The expression of the RUVBL1 component of the R2TP complex correlates with poor prognosis in DLBCL. Pathobiology (2022): 1–11. doi: 10.1159/000520723
18. Li H, Zhou T, Zhang Y, Jiang H, Zhang J, Hua Z. RuvBL1 maintains resistance to TRAIL-induced apoptosis by suppressing c-Jun/AP-1 activity in non-small cell lung cancer. Front Oncol (2021) 11:679243. doi: 10.3389/fonc.2021.679243
19. Liu YJ, Zeng SH, Hu YD, Zhang YH, Li JP. Overexpression of NREP promotes migration and invasion in gastric cancer through facilitating epithelial-mesenchymal transition. Front Cell Dev Biol (2021) 9:746194. doi: 10.3389/fcell.2021.746194
20. Zhang Y, Huang L, Fu H, Smith OK, Lin CM, Utani K, et al. A replicator-specific binding protein essential for site-specific initiation of DNA replication in mammalian cells. Nat Commun (2016) 7:11748. doi: 10.1038/ncomms11748
21. Kim JH, Jeong K, Li J, Murphy JM, Vukadin L, Stone JK, et al. SON drives oncogenic RNA splicing in glioblastoma by regulating PTBP1/PTBP2 switching and RBFOX2 activity. Nat Commun (2021) 12:5551. doi: 10.1038/s41467-021-25892-x
22. Yang X, Wang M, Lin B, Yao D, Li J, Tang X, et al. miR-487a promotes progression of gastric cancer by targeting TIA1. Biochimie (2018) 154:119 – 26. doi: 10.1016/j.biochi.2018.08.006
23. Liao S, Liu T, Yang R, Tan W, Gu J, Deng M. Structure and function of sodium channel Nav1.3 in neurological disorders. Cell Mol Neurobiol (2022). doi: 10.1007/s10571-022-01211-w
24. Thuresson AC, Van Buggenhout G, Sheth F, Kamate M, Andrieux J, Smith HC, et al. Whole gene duplication of SCN2A and SCN3A is associated with neonatal seizures and a normal intellectual development. Clin Genet (2017) 91:106–10. doi: 10.1111/cge.12797
25. Pérez-Martínez A, Valentín J, Fernández L, Hernández-Jiménez E, López-Collazo E, Zerbes P, et al. Arabinoxylan rice bran (MGN-3/Biobran) enhances natural killer cell-mediated cytotoxicity against neuroblastoma in vitro and in vivo. Cytotherapy (2015) 17:601–12. doi: 10.1016/j.jcyt.2014.11.001
26. Chen H, Tan J, Li X, Li H, Wu W, Wu Y, et al. Myeloid and plasmacytoid dendritic cell combined vaccines loaded with heat-treated tumor cell lysates enhance antitumor activity in murine lung cancer. Oncol Lett (2021) 21:90. doi: 10.3892/ol.2020.12351

27. Green MR, Alizadeh AA. Common progenitor cells in mature B-cell malignancies: implications for therapy. Curr Opin Hematol (2014) 21:333–40. doi: 10.1097/moh.0000000000000049
28. Buser L, Bihl M, Rufle A, Mickys U, Tavoriene I, Griskevicius L, et al. Unique composite hematolymphoid tumor consisting of a pro-T lymphoblastic lymphoma and an indeterminate dendritic cell tumor: evidence for divergent common progenitor cell differentiation. Pathobiology (2014) 81:199–205. doi: 10.1159/000365396
29. Tatsumi T, Kierstead LS, Ranieri E, Gesualdo L, Schena FP, Finke JH, et al. Disease-associated bias in T helper type 1 (Th1)/Th2 CD4(+) T cell responses against MAGE-6 in HLA-DRB10401(+) patients with renal cell carcinoma or melanoma. J Exp Med (2002) 196:619–28. doi: 10.1084/jem.20012142
30. Fridman WH, Pagès F, Sautès-Fridman C, Galon J. The immune contexture in human tumours: impact on clinical outcome. Nat Rev Cancer (2012) 12:298–306. doi: 10.1038/nrc3245
31. Raieli S, Di Renzo D, Lampis S, Amadesi C, Montemurro L, Pession A, et al. MYCN drives a tumor immunosuppressive environment which impacts survival in neuroblastoma. Front Oncol (2021) 11:625207. doi: 10.3389/fonc.2021.625207
32. Mukherjee N, Ji N, Hurez V, Curiel TJ, Montgomery MO, Braun AJ,et al. Intratumoral CD56^{bright} natural killer cells are associated with improved survival in bladder cancer. Oncotarget (2018) 9:36492–502. doi: 10.18632/oncotarget.26362
33. de Jonge K, Ebering A, Nassiri S, Maby-El Hajjami H, Ouertatani-Sakouhi H, Baumgaertner P, et al. Circulating CD56^{bright} NK cells inversely correlate with survival of melanoma patients. Sci Rep (2019) 9:4487. doi: 10.1038/s41598-019-40933-8
34. Xu W, Li S, Li M, Yang X, Xie S, Lin L, et al. Targeted elimination of myeloid-derived suppressor cells via regulation of the STAT pathway alleviates tumor immunosuppression in neuroblastoma. Immunol Lett (2021) 240:31–40. doi: 10.1016/j.imlet.2021.09.011
35. Belounis A, Ayoub M, Cordeiro P, Lemieux W, Teira P, Haddad E, et al. Patients' NK cell stimulation with activated plasmacytoid dendritic cells increases dinutuximab-induced neuroblastoma killing. Cancer Immunol Immunother (2020) 69:1767–79. doi: 10.1007/s00262-020-02581-0
36. Xu L, Wang X, Wan J, Li T, Gong X, Zhang K, et al. Sonic Hedgehog pathway is essential for neuroblastoma cell proliferation and tumor growth. Mol Cell Biochem (2012) 364:235–41. doi: 10.1007/s11010-011-1222-6
37. Gershon TR, Shiraz A, Qin LX, Gerald WL, Kenney AM, Cheung NK. Enteric neural crest differentiation in ganglioneuromas implicates Hedgehog signaling in peripheral neuroblastic tumor pathogenesis. PLoS One (2009) 4:e7491. doi: 10.1371/journal.pone.0007491
38. Eckerle I, Muth D, Batzler J, Henrich KO, Lutz W, Fischer M, et al. Regulation of BIRC5 and its isoform BIRC5-2B in neuroblastoma. Cancer Lett (2009) 285:99–107. doi: 10.1016/j.canlet.2009.05.007
39. Lamers F, van der Ploeg I, Schild L, Ebus ME, Koster J, Hansen BR, et al. Knockdown of survivin (BIRC5) causes apoptosis in neuroblastoma via mitotic catastrophe. Endocr Relat Cancer (2011) 18:657–68. doi: 10.1530/erc-11-0207

40. Liao X, Qian X, Zhang Z, Tao Y, Li Z, Zhang Q, et al. ARV-825 demonstrates antitumor activity in gastric cancer via MYC-targets and G2M-checkpoint signaling pathways. Front Oncol (2021) 11:753119. doi: 10.3389/fonc.2021.753119

Figures

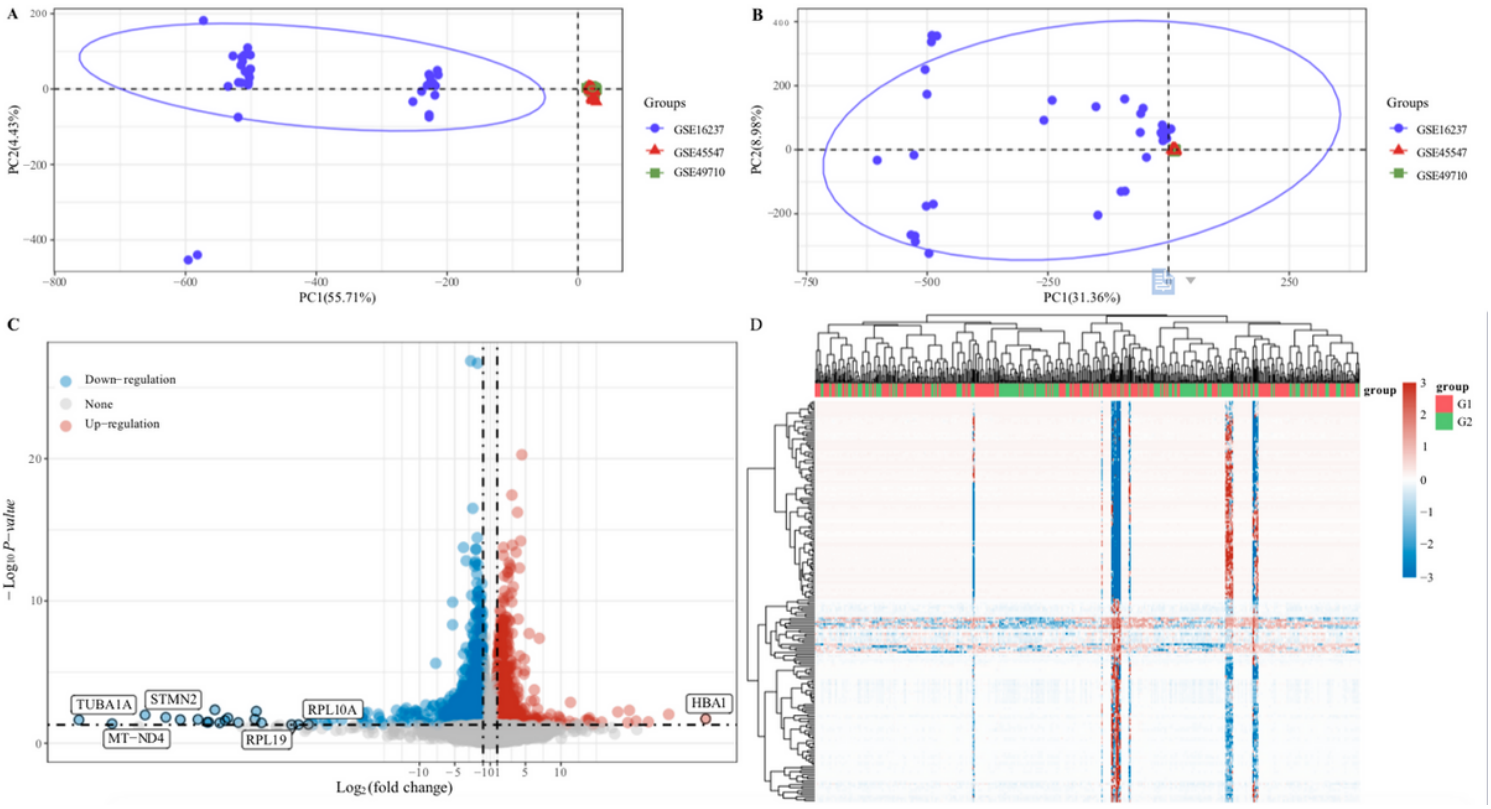

Figure 1

A. PCA results before batch removal for multiple data sets. Different colors represent different data sets. The three data sets are separated without any intersections.

B. PCA results after batch removal, showing the intersections of the three data sets, which can be used as a single batch for subsequent analyses.

C. Volcano plots using as criteria log2FC >3 and adjusted P 0.05. The red points represent significantly over-expressed and the blue points represents significantly under-expressed mRNAs.

D. Hierarchical clustering analysis of mRNAs differentially expressed in tumor and normal tissues.

Figure 2

A. Forest plot of 53 prognosis-related genes in DEGs

B. Results of lasso regression analysis showing the compression path diagram.

C. Selected feature coefficients of lasso regression analysis, as represented by lambda parameters.

D. Forest plot based on the results of lasso regression analysis.

E. ROC curves of the 12 prognosis related genes

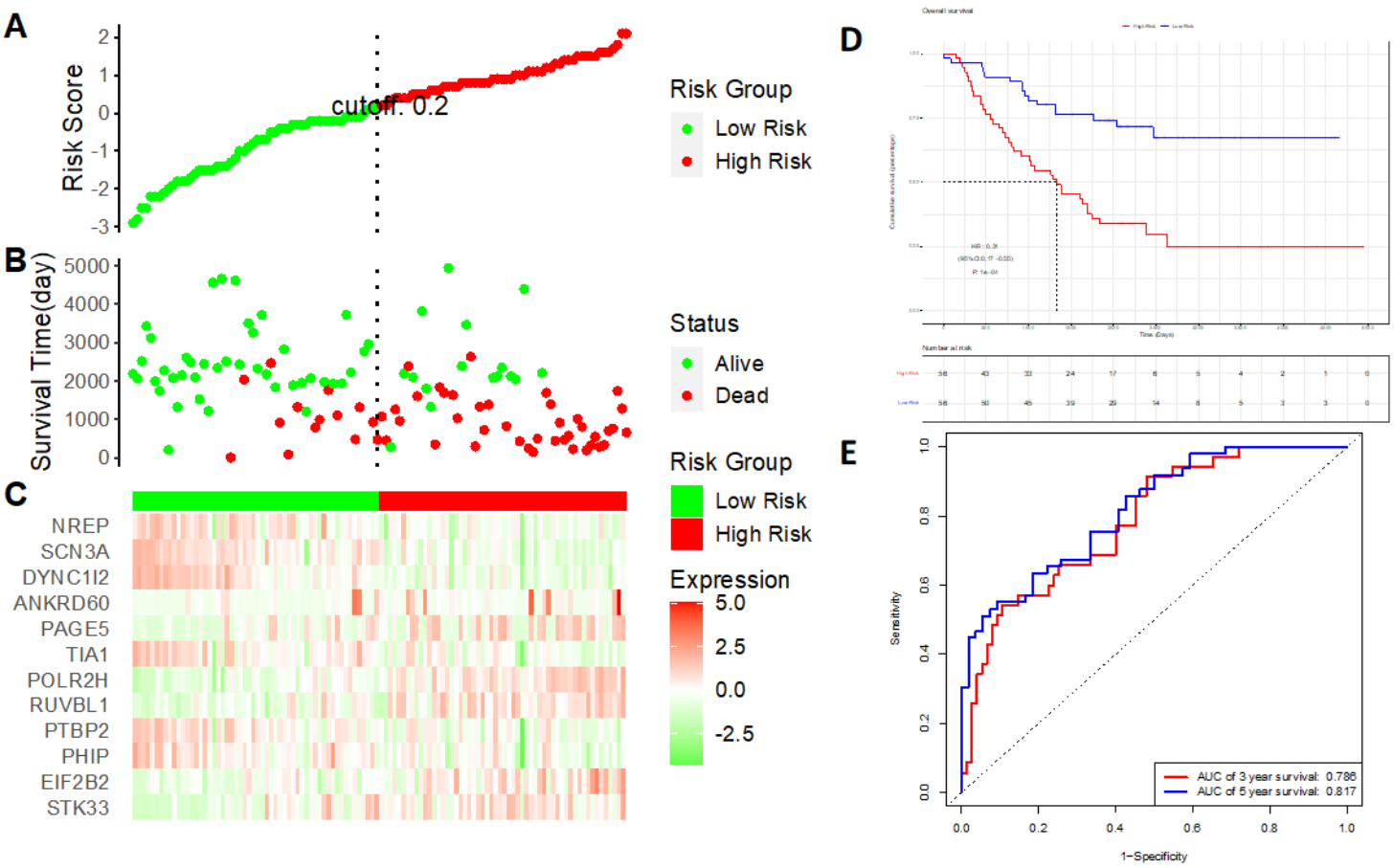

Figure 3

A. Division of patients into a high-risk and a low-risk group based on the median risk score of the prognostic model.

B. Relationship between patient survival and risk scores.

C. Relationship between level of expression of each gene and risk score.

D. Kaplan-Meier analysis of overall survival in the high- and low-risk groups

E. ROC curves of the survival model, showing 3-year and 5-year AUCs of 78.6% and 81.7%, respectively.

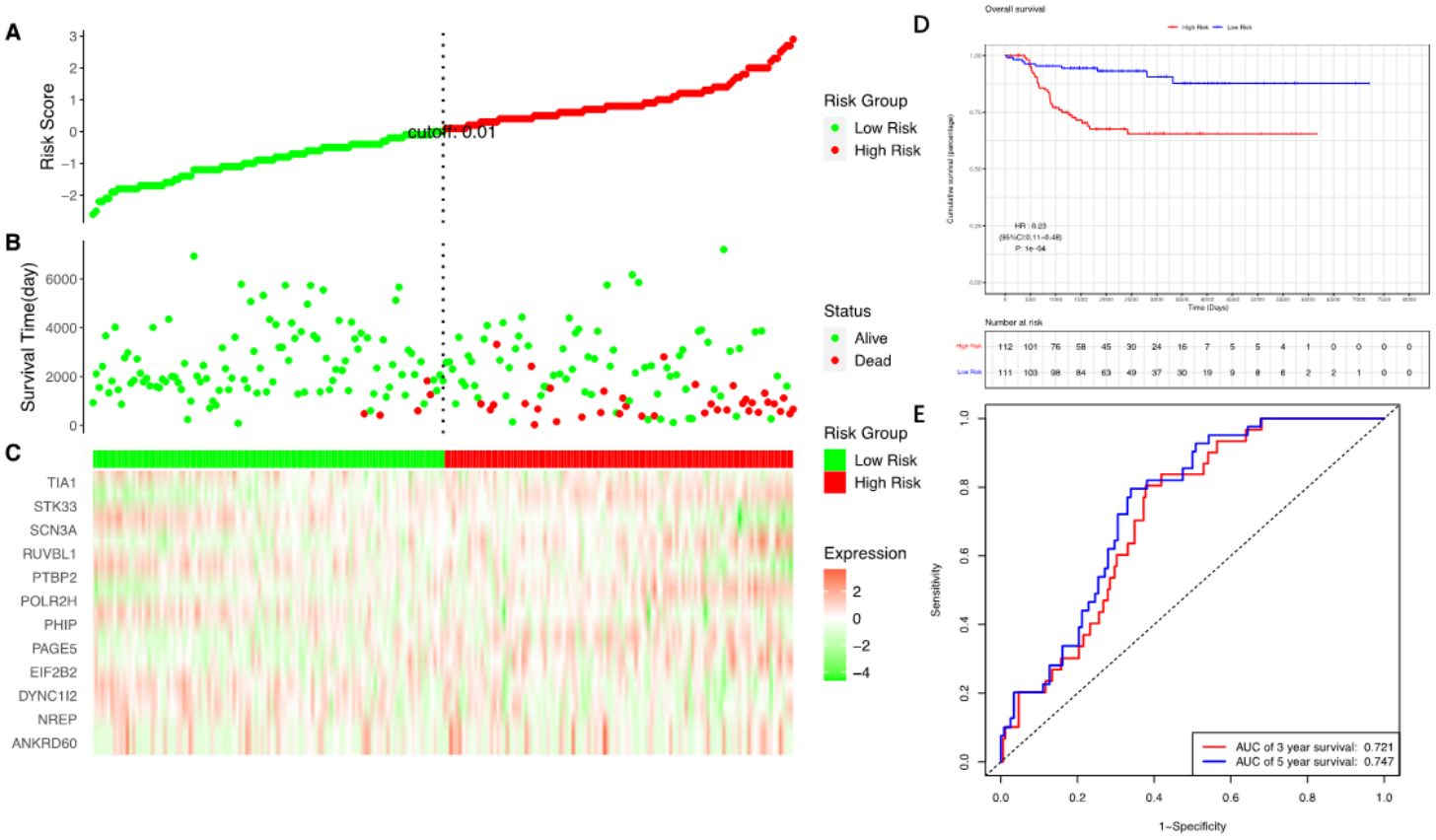

Figure 4

A. Division of patients into a high-risk group and a low-risk group based on the median risk score of the prognostic model

B. Relationship between patient survival and risk scores.

C. Relationship between level of expression of each gene and risk score.

D. Kaplan-Meier analysis of overall survival in the high- and low-risk groups

E. ROC curves of the survival model, showing 3-year and 5-year AUCs of 72.1% and 74.7%, respectively.

A

	HR	lower 95%CI	upper 95%CI	pvalue
risk_score	1.664	1.417	1.955	0.000
Gender	0.801	0.434	1.476	0.476
age	16.014	2.201	116.519	0.006
MYCN	1.735	0.901	3.342	0.099
Hyperdiploid	0.424	0.230	0.784	0.006
MKI	1.771	1.205	2.602	0.004
COG	8.643	1.437	51.998	0.018

B

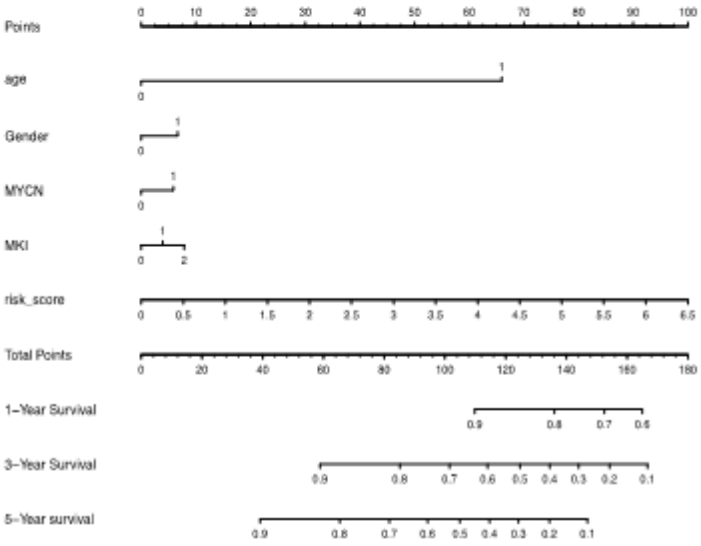

C

Figure 5

A. Results of multivariate Cox survival analysis.

B. Nomogram based on the results of multivariate Cox survival analysis

C. Calibration curve for the nomogram

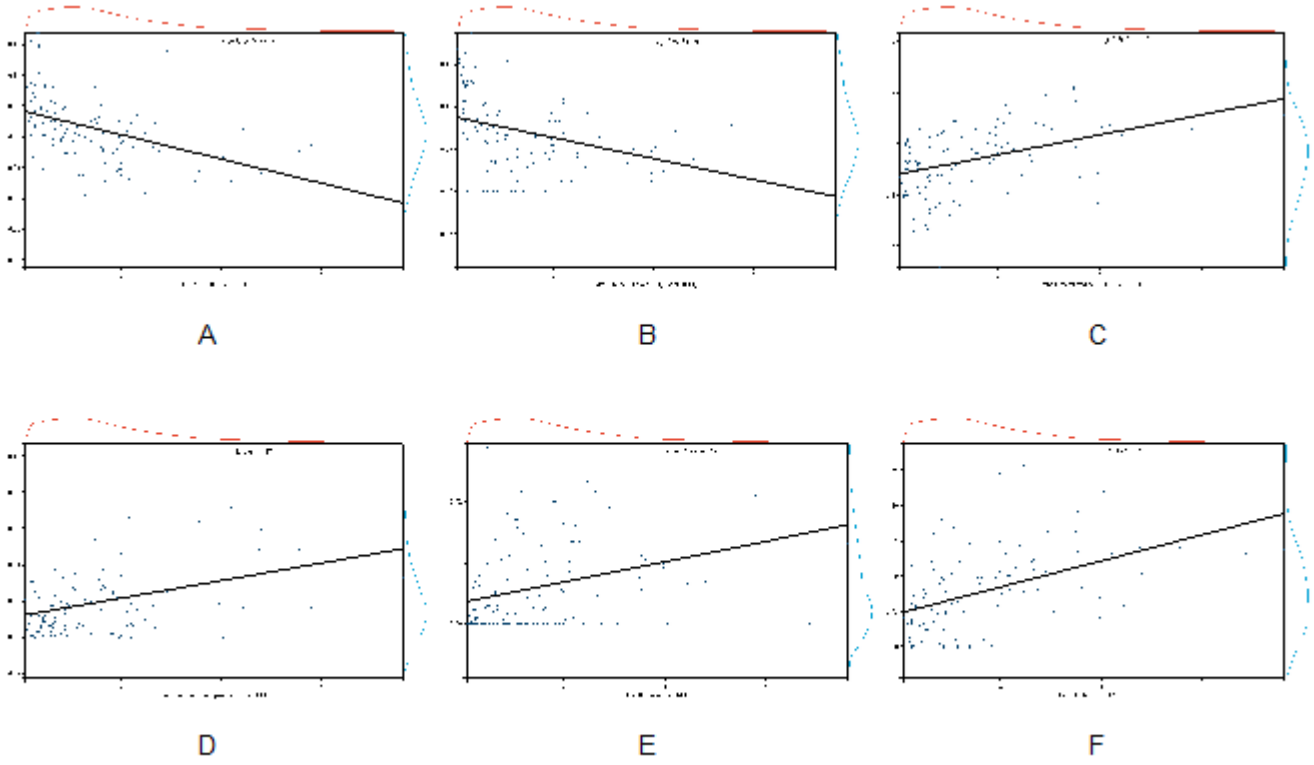

Figure 6

Correlations between risk score and immune cell infiltration into NBs. (A) NK cell (R=-0.50, P<0.01), (B) myeloid dendritic cells (R=-0.41, P<0.01), (C) uncharacterized cells (R=0.42, P<0.01), (D) common lymphoid progenitor cells (R=0.37, P<0.01), (E) B cells (R=0.35, P<0.01), (F) CD4+ Th1 T cells (R=0.49, P<0.01).

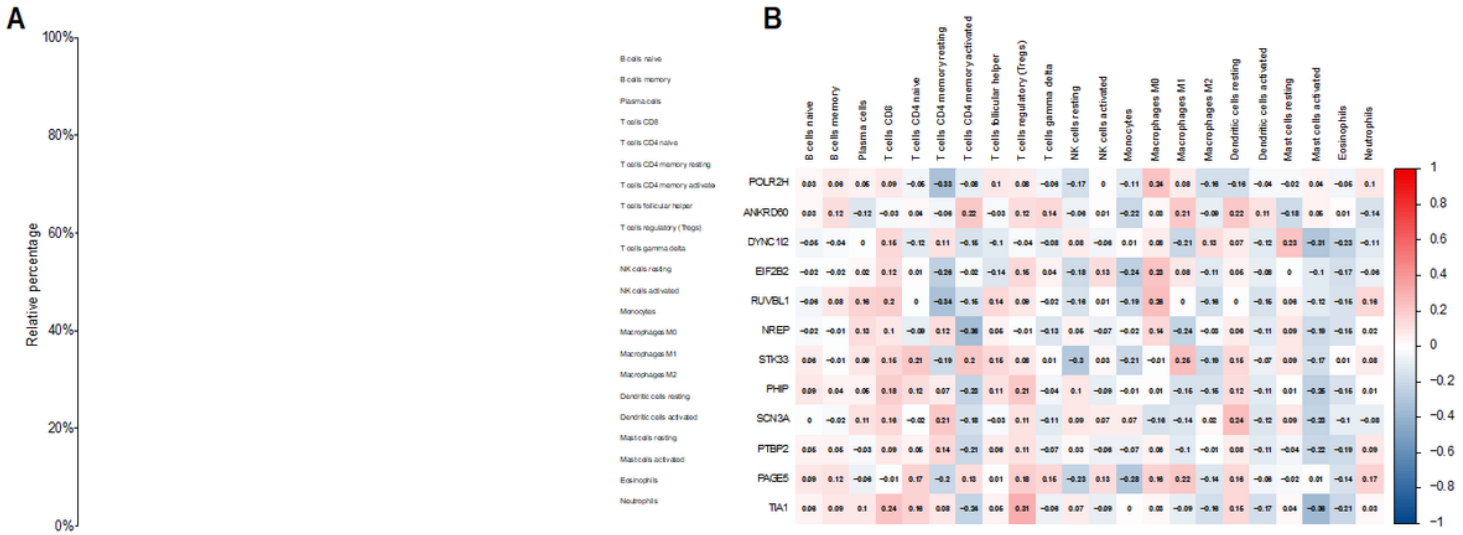

Figure 7

A. CIBERSORT results in 142 patients from the TARGET dataset.

B. Pearson correlation between CIBERSORT immune cells and 12 prognosis-related genes.

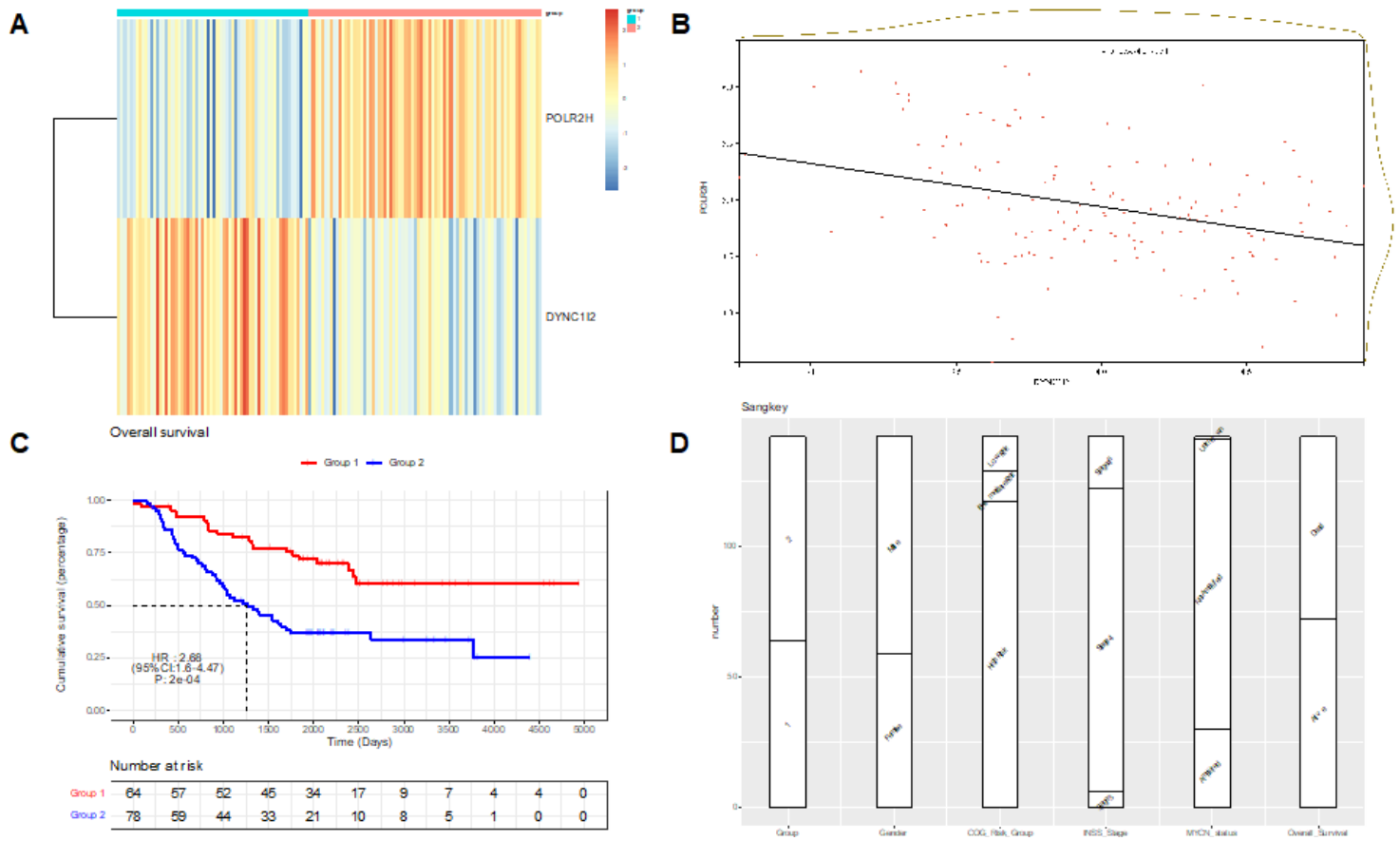

Figure 8

A. Division of TARGET-NBL patients into two clusters based on tumor expression of POLR2H and DYNC1I2.

B. Association between POLR2H and DYNC1I2 expression

C. Kaplan-Meier analysis of overall survival curve of patients in the two clusters

D. Sankey diagram showing the relationship between clinical features and prognosis of the two clusters

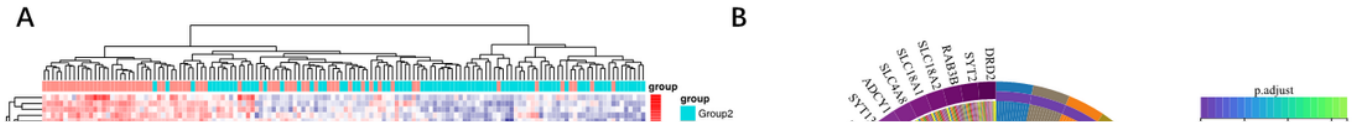

Figure 9

A. Heatmap of differentially expressed genes. Colors represent trends in expression

B. Circle graph showing the results of GO enrichment analysis

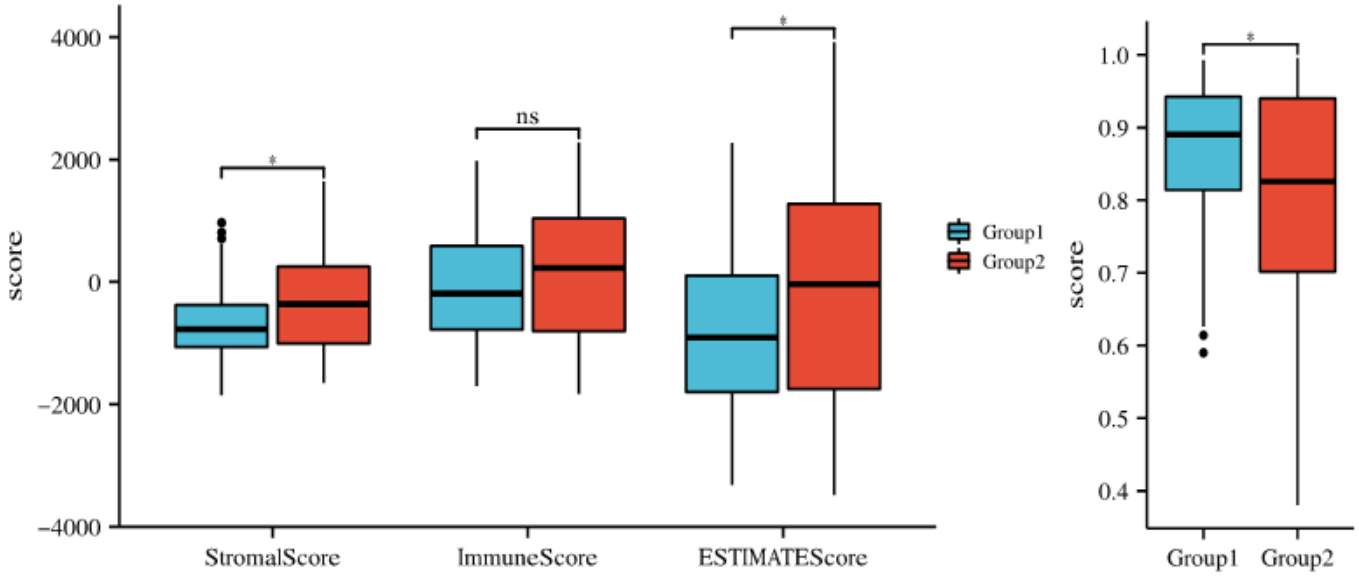

Figure 10

Stromal score, immune score, and ESTIMATE score in clusters 1 and 2.

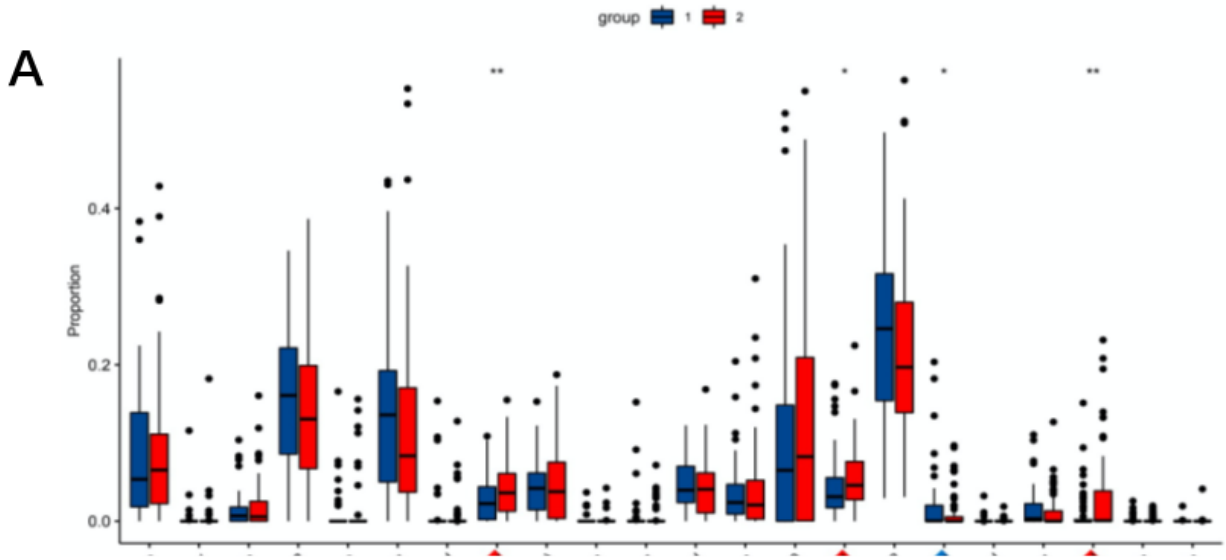

Figure 11

A. Proportions of immune cells in clusters 1 and 2.

B. Expression of immune cells in clusters 1 and 2.

ns, not significant, *P < 0.05, **P < 0.01, ***P < 0.001.

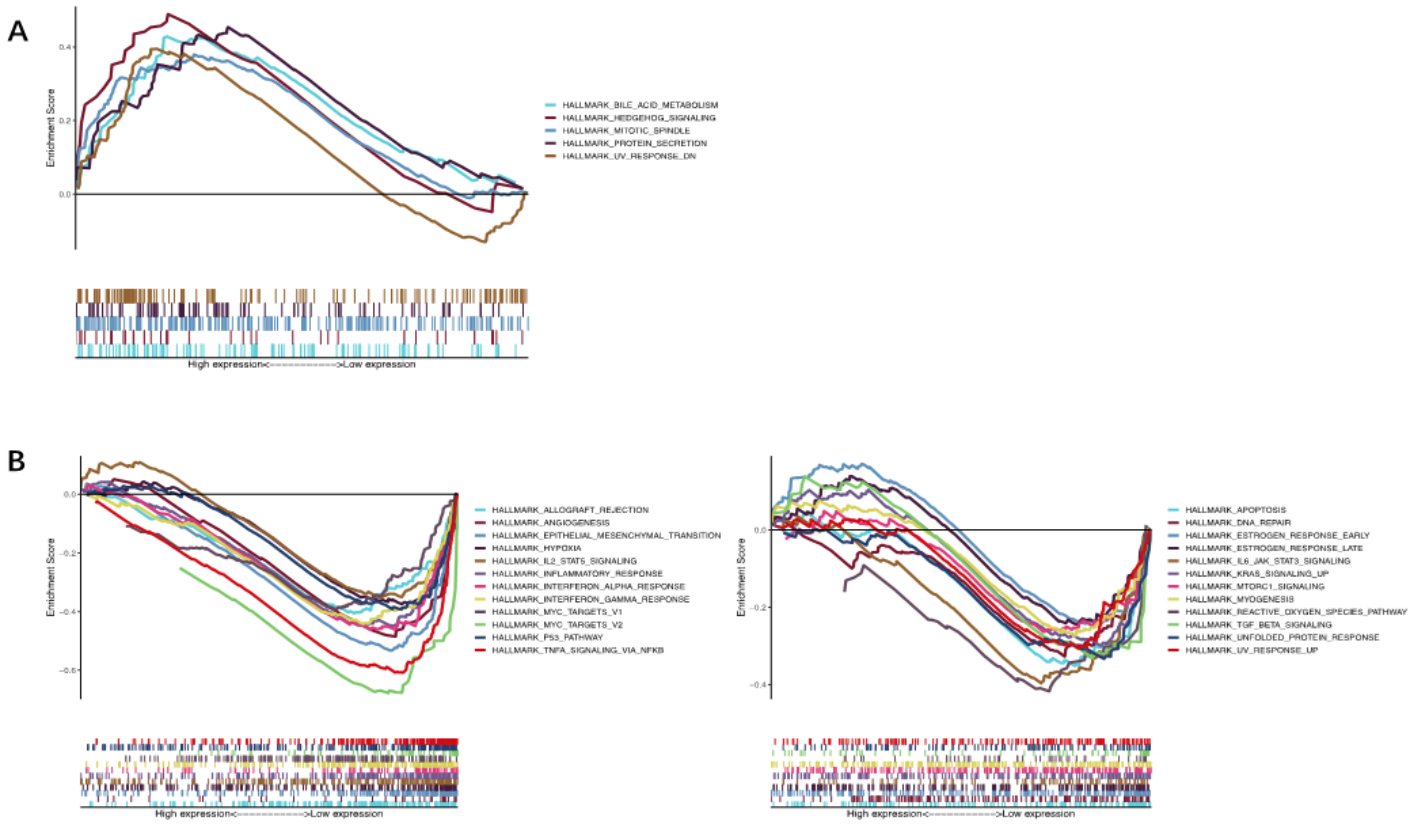

Figure 12

TARGET-NBL GSEA results of functional enrichment of immune characteristics in (A) Cluster 1 and (B) Cluster 2 of patients with NB.

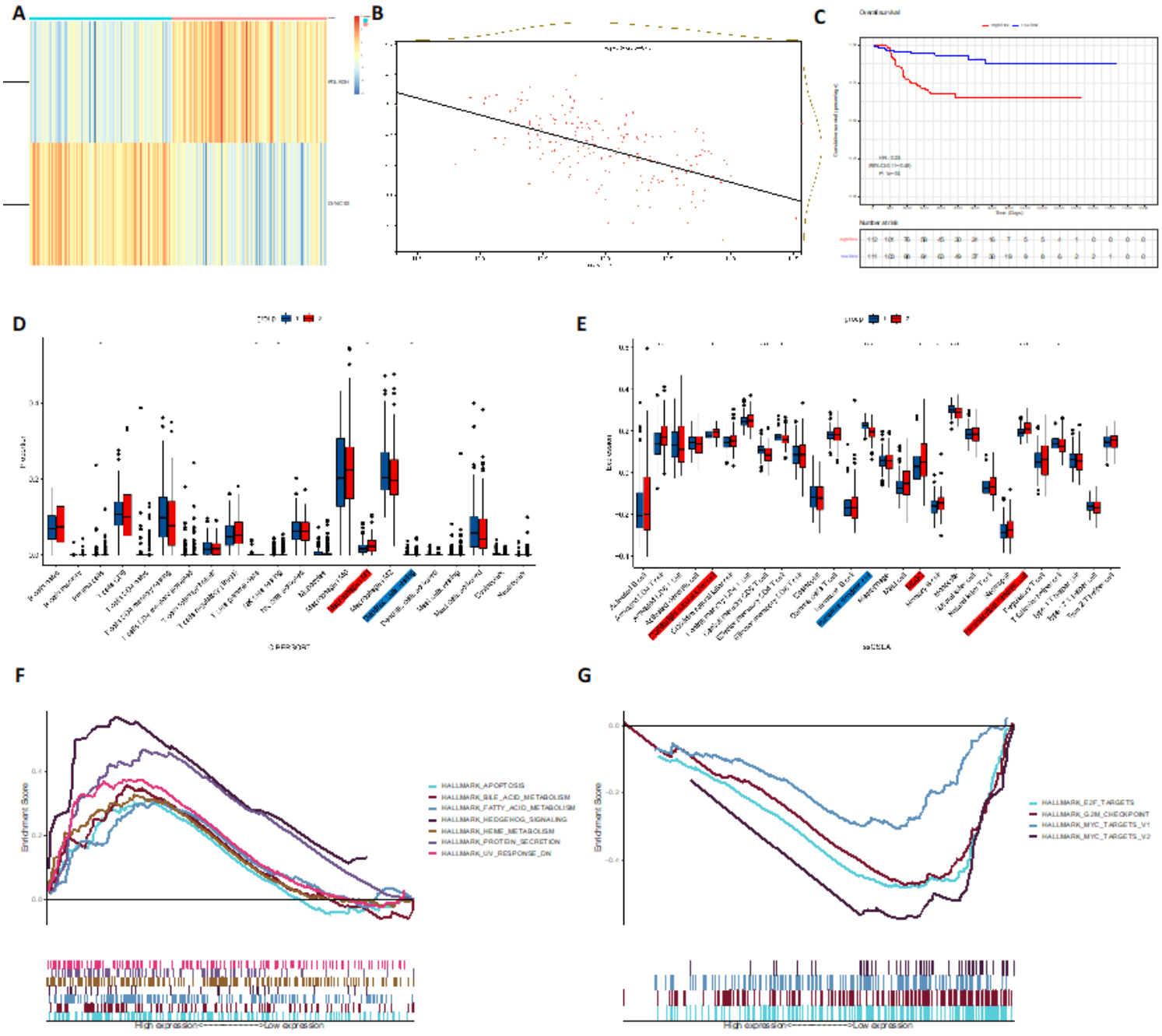

Figure 13

A. Division of patients in the E-MTAB-8248 dataset into two clusters based on POLR2H and DYNC1I2 expression.

B. Association between POLR2H and DYNC1I2 expression in the E-MTAB-8248 dataset.

C. Kaplan-Meier analysis of overall survival of patients in the two clusters of the E-MTAB-8248 dataset.

D. Proportion of immune cells in patients in the E-MTAB-8248 dataset.

E. Expression of immune cells in patients in the E-MTAB-8248 dataset.

ns, not significant, *P < 0.05, **P < 0.01, ***P < 0.001.

F. GSEA analysis of E-MTAB-8248 dataset Group 1

G. GSEA analysis of E-MTAB-8248 dataset Group 2

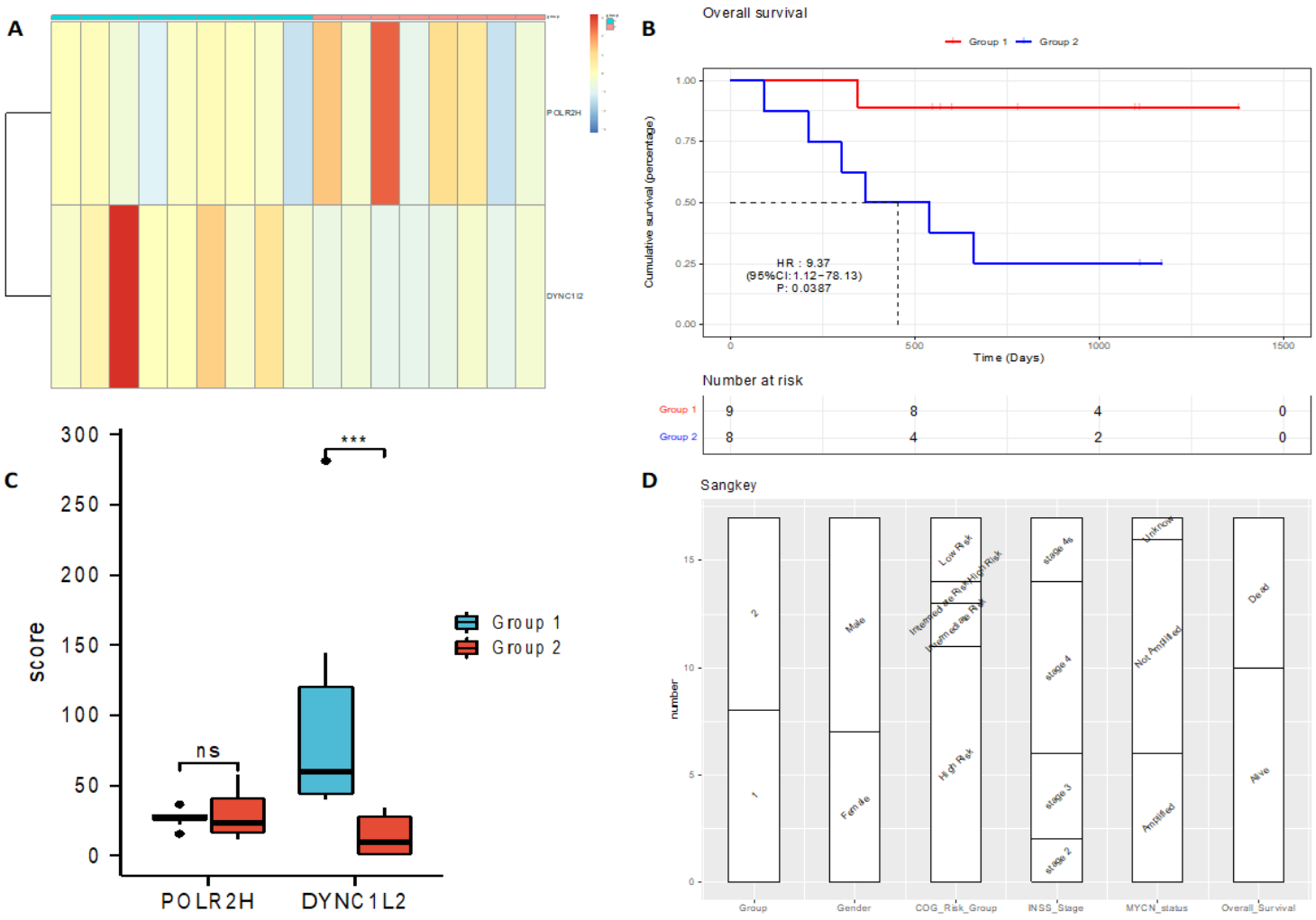

Figure 14

A. Division of patients into two clusters based on their expression of POLR2H and DYNC1I2

B. Kaplan-Meier analysis of overall survival in the two groups

C. RT-qPCR analysis of POLR2H and DYNC1I2 expression in NB tissues. ns, not significant, ***P < 0.001.

D. Sankey diagram showing the relationship between clinical features and prognosis in the two groups.